Modeling pion physics in the ϵ-regime of two-flavor QCD using strong coupling lattice QED

D. J. Cecile and Shailesh Chandrasekharan

Department of Physics, Box 90305, Duke University,

Durham, North Carolina 27708, USA

arXiv:0708.0558v1 [hep-lat] 3 Aug 2007

Abstract

In order to model pions of two-flavor QCD we consider a lattice field theory involving two flavors of staggered quarks interacting strongly with $U(1)$ gauge fields. For massless quarks, this theory has an $SU_L(2) \times SU_R(2) \times U_A(1)$ symmetry. By adding a four-fermion term we can break the $U_A(1)$ symmetry and thus incorporate the physics of the QCD anomaly. We can also tune the pion decay constant F, to be small compared to the lattice cutoff by starting with an extra fictitious dimension, thus allowing us to model low energy pion physics in a setting similar to lattice QCD from first principles. However, unlike lattice QCD, a major advantage of our model is that we can easily design efficient algorithms to compute a variety of quantities in the chiral limit. Here we show that the model reproduces the predictions of chiral perturbation theory in the ϵ-regime.

I. INTRODUCTION

One of the outstanding problems in lattice QCD is to compute low energy hadronic observables, which are dominated by the physics of light quarks, with controlled errors. Unfortunately, with current algorithms it is difficult to perform calculations at realistic quark masses. In particular, one would like to have light pions of mass 140 Mev, which means $\frac{m_l}{m_s} \sim \frac{1}{25}$, where m_l refers to the average up and down quark masses and m_s refers to the strange quark mass. In practice the lightest pions with current algorithms can reach about 250-300 MeV with Wilson type fermions [1] and slightly lighter with staggered fermions. For example the MILC group has attained $\frac{m_l}{m_s} \sim \frac{1}{8}$ with staggered fermions while $\frac{m_l}{m_s} > \frac{1}{2}$ is common [2]. Given that calculations are usually performed at unphysically large quark masses, chiral extrapolations, based on chiral perturbation theory, are used to obtain results at realistic quark masses. However, for such an approach to be reliable, we must know the range of quark masses over which the chiral expansion used in the extrapolation is valid. Unfortunately, this is not yet well understood.

One way to check if chiral extrapolations are reliable is to verify them in qualitatively distinct regimes. Fortunately, while there are many such regimes depending on the values of the pion masses and the physical box sizes, the most popular examples are the p-regime and the ϵ-regime. Interestingly, in all the regimes the extrapolation formulas depend on the same low energy constants that describe the chiral Lagrangian. Hence if the data from a lattice calculation can be fit in both the regimes with the same low energy constants one would gain more confidence in the extrapolations. As far as we know such comparisons have not yet been made in the context of lattice QCD. In fact, although chiral perturbation theory is a widely understood and accepted tool, much less effort has gone into describing the low energy physics of a fundamental lattice field theory using the chiral Lagrangian. Apart from lattice QCD, as far as we know, the only known example where lattice results were understood with chiral perturbation theory was in the context of the non-linear sigma models [3, 4, 5] and quantum spin systems [6]. However, even in such studies comparison between the p-regime and the ϵ-regimes were never made. Further, these studies are some what outdated given the advances in computing resources. More such studies and with simpler models that resemble QCD closely may teach us more about chiral extrapolations. Motivated by this, we introduce and study a lattice field theory model of pions in two-flavor

QCD.

Our model is nothing but strongly coupled lattice QED with two flavors of staggered fermions. This model exhibits the same symmetries as two flavor QCD and was recently used to study the chiral phase transition [7]. The strong coupling limit was studied considerably in the eighties [8, 9, 10, 11, 12, 13, 14, 15, 16, 17] because some of the qualitative physics remains despite this limit suffering from the worst lattice artifacts. In fact, even a $U(1)$ gauge theory exhibits confinement and chiral symmetry breaking in the strong coupling limit. Notice further that the taste symmetry of continuum staggered fermions is irrelevant since it is maximally broken at strong couplings. The relevant symmetry is due to the two flavors and resembles QCD closely. Thus, our model allows us to model pion physics from a fundamental lattice field theory, very similar to QCD.

Since the pion is the lightest QCD bound state and plays a crucial role in chiral symmetry breaking, even a qualitative description of it from first principles may prove useful. However, unless we find a way to fine tune our model, the pion decay constant F (defined here in the chiral limit), is naturally close to the cutoff. Thus, the low energy pion physics in our model may be described by a chiral Lagrangian that contains information about lattice artifacts. In order to circumvent this problem, we define our model in $d+1$ dimensions where $d=4$ is the space time dimensions. The extra dimension plays the role of a fictitious temperature which allows us to tune F to values much smaller than the cut-off. Thus, we can still explore "continuum-like" physics even in the strong coupling limit.

In addition to its similarity with QCD, another important motivation for studying the above model is that the gauge dependent degrees of freedom can be integrated over, which significantly simplifies the theory. Further, a new class of algorithms, called *the Directed Path Algorithm*, allows us to study the chiral limit very efficiently [18]. Here we extend the algorithm to our model and show that the results in the chiral limit agree with predictions in the ϵ-regime. A preliminary version of this work can be found in [19].

II. MODEL AND SYMMETRIES

The Euclidean space action of the model we consider is given by (note that the usual factor of $\frac{1}{2}$ in the fermion kinetic term has been absorbed into the fields):

$$S = -\sum_x \sum_{\mu=1}^{d+1} \eta_{\mu,x} \left[\mathrm{e}^{i\phi_{\mu,x}} \overline{\psi}_x \psi_{x+\hat{\mu}} - \mathrm{e}^{-i\phi_{\mu,x}} \overline{\psi}_{x+\hat{\mu}} \psi_x \right] - \sum_x \left[m \overline{\psi}_x \psi_x + \frac{\tilde{c}}{2} \left(\overline{\psi}_x \psi_x \right)^2 \right], \qquad (1)$$

where x denotes a lattice site on a $d+1$ dimensional hyper-cubic lattice $L_t \times L^d$. Here L_t represents a fictitious time direction and will be used to tune F, the non-perturbative physical mass scale, to be small compared the lattice cutoff. On the other hand L^d will be the usual Euclidean space-time box. $\overline{\psi}_x$ and ψ_x are two component Grassmann fields that represent the two quark (u, d) flavors of mass m, and $\phi_{\mu,x}$ is the compact $U(1)$ gauge field through which the quarks interact. Here $\mu = 1, 2, ..., d, d+1$ runs over the $d+1$ directions. The $\mu = 1$ direction will denote the fictitious temperature direction, while the remaining directions represent Euclidean space-time. The usual staggered fermion phase factors $\eta_{\mu,x}$ obey the relations: $\eta_{1,x}^2 = T$ and $\eta_{i,x}^2 = 1$ for $i = 2, 3, ..., d+1$. The parameter T controls the fictitious temperature and will be used to tune to the continuum limit ($F \ll 1$). The coupling $\tilde{c}$ will set the strength of the anomaly.

When $\tilde{c}, m = 0$, the action exhibits a global $SU_L(2) \times SU_R(2) \times U_A(1)$ symmetry like $N_f = 2$ QCD. To see this it is first useful to note that every lattice site can be classified as an *even* or *odd* site. Then it is easy to see that the action is invariant under the following transformations: $\overline{\psi}_o \to \overline{\psi}_o V_L^\dagger \exp(i\phi), \psi_o \to \exp(i\phi) V_R \psi_o, \overline{\psi}_e \to \overline{\psi}_e V_R^\dagger \exp(-i\phi), \psi_e \to \exp(-i\phi) V_L \psi_e$. Here V_L and V_R are $SU(2)$ matrices and can be parametrized by: $\exp(i\vec{\theta} \cdot \vec{\sigma})$ where σ_i is a Pauli matrix that acts on the flavor space. At $\tilde{c} \neq 0$, $U_A(1)$ is explicitly broken and the action is invariant under $SU_L(2) \times SU_R(2) \times Z_2$. Thus, the coupling $\tilde{c}$ induces the effects of the anomaly. Further at $m \neq 0$, it is necessary to set $V_L = V_R$ for the action to remain invariant. Thus, with a mass term the chiral symmetry $SU_L(2) \times SU_R(2)$ is explicitly broken down to $SU_V(2)$. In order to mimic the real world with u,d quarks we need to set $\tilde{c} \neq 0$ and $m \neq 0$. Thus, our model has the same chiral symmetry as $N_f = 2$ QCD. Further, based on previous mean field strong coupling calculations [10], we expect that the symmetry breaking pattern is also similar to full QCD.

III. MONOMER-DIMER-PION LOOP-INSTANTON REPRESENTATION

The partition function of our model is equivalent to that of a classical statistical mechanics model involving configurations made up of gauge invariant objects such as monomers, dimers, pion loops and instantons [20]. We call these MDPI configurations and denote the set of all such configurations by $\mathcal{K}$. Each MDPI configuration is characterized by three site variables $I(x), n_u(x), n_d(x)$ and three bond variables $\pi^u_\mu(x), \pi^d_\mu(x), \pi^1_\mu(x)$. Here $n_u(x)$ is the number of $\overline{u}u$ monomers, $n_d(x)$ the number of $\overline{d}d$ monomers and $I(x)$ the number of instantons (or $\overline{u}u\overline{d}d$ double-monomers) associated with the site x. On the other hand $\pi^u_\mu(x)$ denotes the number of $\overline{u}u\overline{u}u$ dimers, $\pi^d_\mu(x)$ the number of $\overline{d}d\overline{d}d$ dimers, and $\pi^1_\mu(x)$ the number of oriented ($\overline{u}d\overline{d}u$ or $\overline{d}u\overline{u}d$) dimers that live on the bond connecting x and $x+\hat{u}$. In our notation $\pi^u_{-\mu}(x) = \pi^u_\mu(x-\hat{\mu})$ and similarly for other bond variables. The allowed values for these variables are:

$$I(x) = 0, 1 \quad n_d(x) = 0, 1 \quad n_u(x) = 0, 1 \quad \pi^d_\mu(x) = 0, 1 \quad \pi^u_\mu(x) = 0, 1 \quad \pi^1_\mu(x) = -1, 0, 1 \quad (2)$$

Note that $n_u(x) = n_d(x) = 1$ is not allowed since it is absorbed into $I(x)$. Due to the Grassmann nature of the fermion fields the following constraints must also be satisfied at each site x:

$$\sum_\mu \pi^1_\mu(x) \;=\; 0 \tag{3a}$$

$$2I(x) + \sum_\mu \Big[\pi^u_\mu(x) + \pi^d_\mu(x) + n^u(x) + n^d(x)\Big] + \sum_\mu \big|\pi^1_\mu(x)\big| \;=\; 2 \tag{3b}$$

$$n_u(x) + \sum_\mu \Big[\pi^u_\mu(x) - \pi^d_\mu(x)\Big] - n_d(x) \;=\; 0 \tag{3c}$$

where the sum over μ goes over $\pm 1, ... \pm (d+1)$. Fig.(1) gives an illustration of an MDPI configuration in $1+1$ dimensions.

Note that $I(x) = 1$ on a site x breaks the $U_A(1)$ symmetry but not the $SU_L(2) \times SU_R(2)$ symmetry and hence it is called an *instanton*. In addition to these, each configuration can contain *neutral pion-loops* of alternating $\overline{u}u\overline{u}u$ and $\overline{d}d\overline{d}d$ dimers or *charged pion-loops* of $\overline{u}d\overline{d}u$ (or $\overline{d}u\overline{u}d$) dimers. Neutral pions can also form open strings at non-zero m with $\overline{u}u$ or $\overline{d}d$ monomers at the ends, while charged pions cannot form such open strings in our model. Note also that if a bond consists of two dimers (double bond) it can be considered both as a neutral pion-loop or a charged pion-loop. Finally, it is useful to recognize that charged

pion-loops are naturally oriented while neutral pion-loops are not. On the other hand it is possible to give an orientation to the neutral pion-loops also. Here we will assume that a $\overline{u}u\overline{u}u$ dimer on a forward bond from an even site and a $\overline{d}d\overline{d}d$ dimer on a forward bond from an odd site are considered oriented forward. Similarly a $\overline{u}u\overline{u}u$ dimer on a forward bond from an odd site and a $\overline{d}d\overline{d}d$ dimer on a forward bond from an even site are considered oriented backward. With this convention it is clear that neutral pion-loops are also oriented. This will be useful when constructing the algorithm. If we define $c \equiv \tilde{c} + m^2$, the partition function is given by:

$$Z = \sum_{[\mathcal{K}]} \prod_x m^{n_d(x)} m^{n_u(x)} c^{I(x)}. \tag{4}$$

where the sum includes all allowed MDPI configurations.

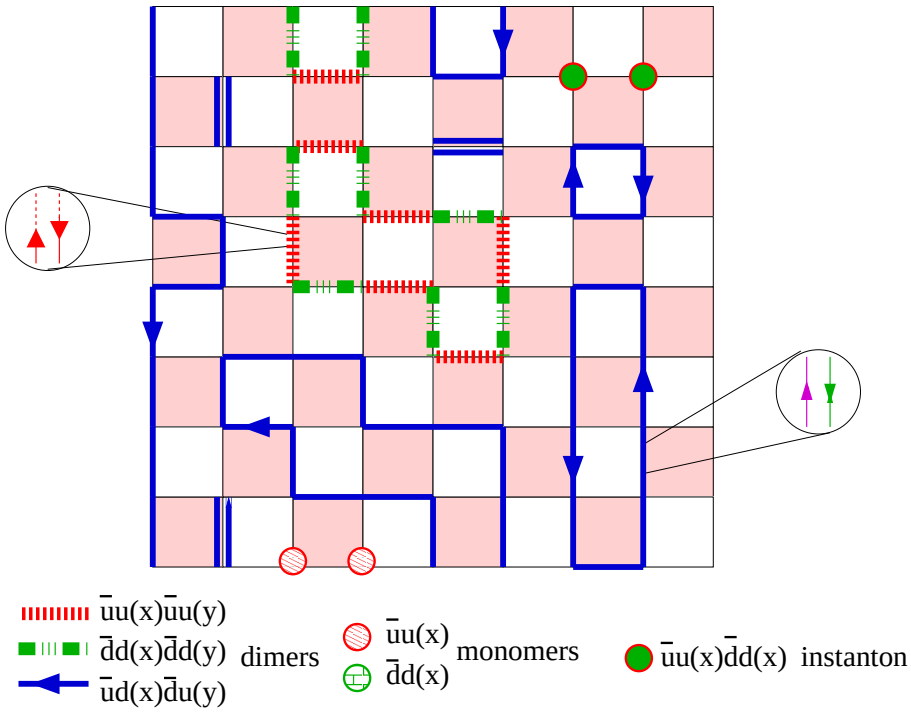

FIG. 1: An example of a 2×2 lattice configuration as discussed in the text.

IV. ALGORITHM

Since the partition function in Eq. (4) is a sum over positive definite weights, a Monte-Carlo algorithm can be used to sample the MDPI configurations $\mathcal{K}$. We have extended the

work of [18, 21] and constructed the algorithm. It is comprised of four updates : a $u \leftrightarrow d$ *flip*, a *loop swap*, and a *directed-path mass update* and a *directed-path fixed-monomer update*. While each update by itself satisfies detailed balance, one needs a combination of these updates to ensure ergodicity. The first three updates are sufficient to ensure ergodicity in general. The fixed monomer update in combination with the flip and the swap allows us to calculate quantities in a fixed monomer sector which will be useful in some of our results. We now discuss each update in detail.

The $u \leftrightarrow d$ flip update This update changes a u quark to a d quark and vice-versa on a pion loop or string. Thus, a $\overline{u}u\overline{u}u$ dimer becomes a $\overline{d}d\overline{d}d$ dimer and vice-versa or a $\overline{u}d\overline{d}u$ dimer becomes a $\overline{d}u\overline{u}d$ dimer and vice-versa. Similarly a $\overline{u}u$ monomer becomes a $\overline{d}d$ monomer. The complete update is as follows:

1. Let V denote the set of all lattice sites. A lattice site $x_0 \in V$ is selected randomly.

2. If x_0 is part of a pion loop or a string, the $u \leftrightarrow d$ flip is performed on all dimers and monomers associated with the loop or string. The update then ends.

3. If x_0 is part of an instanton or a double dimer, the update ends.

Because the configuration before and after the update have equal weights, this update automatically satisfies detailed balance.

Loop swap update. This update swaps a neutral pion-loop into a charged pion-loop and vice-versa. The complete update is as follows:

1. A lattice site $x_0 \in V$ is selected randomly.

2. If x_0 is part of a neutral pion-loop, the complete loop is changed into a charged pion-loop and vice-versa. The update then ends.

3. If x_0 is not part of a loop, the update ends.

Again, because neutral and charged pion-loops have equal weights, this update automatically satisfies detailed balance.

Directed-path mass update. This update is more complex and can create and destroy monomers and instantons while at the same time it can change the shape of the pion loops. We construct and use two types of directed-path update that differ on the sites they are

allowed to touch. The *charged-pion directed path update* can only touch sites containing either charged pion-loops (including double dimers) and instantons, while the *neutral-pion directed path update* can only touch sites containing neutral pion-loops (including double dimers), instantons and monomers. Since the rules of the update are almost the same we will discuss them together. We will call the set of sites a particular update is allowed to touch as $\mathcal{C}$.

To understand the directed path update it is useful to think of the MDPI configurations as constructed with oriented objects. As we have already discussed above every loop is oriented. Open strings of neutral pions are also oriented with an incoming monomer and an outgoing monomer at the two ends. An instanton is also an oriented string of zero length with a forward and a backward monomer on the same site. A forward monomer is oriented into the $\mu = 0$ direction and a backward monomer is oriented from the $\mu = 0$ direction. Thus, each MDPI configuration naturally gives every site a forward and a backward direction. The directed-path update essentially updates these directions on the sites it touches.

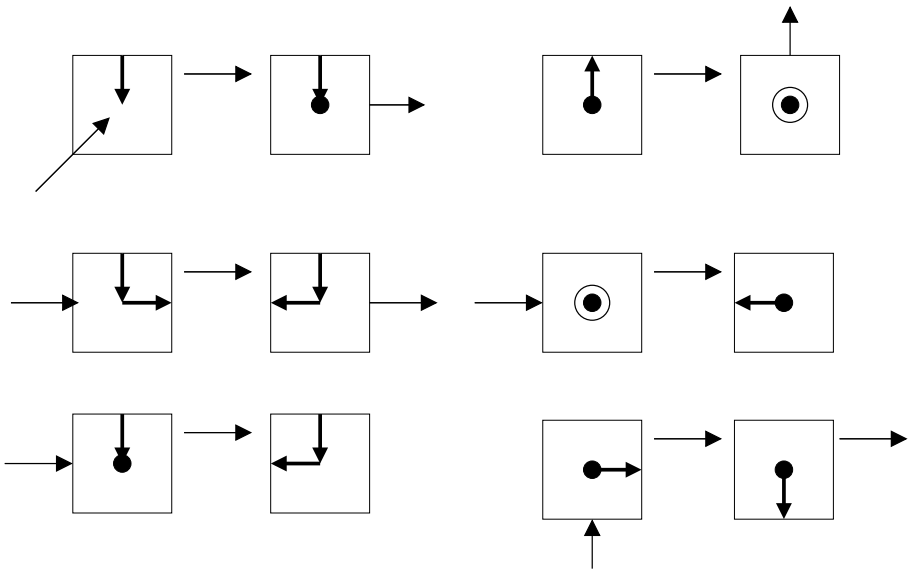

FIG. 2: Examples of the active update at a site. The absence of an outgoing arrow implies that the update remains on the site.

The update consists of two parts: an *active update* and a *passive update*. During an *active update* one replaces the forward direction μ at the site x by the direction ν through

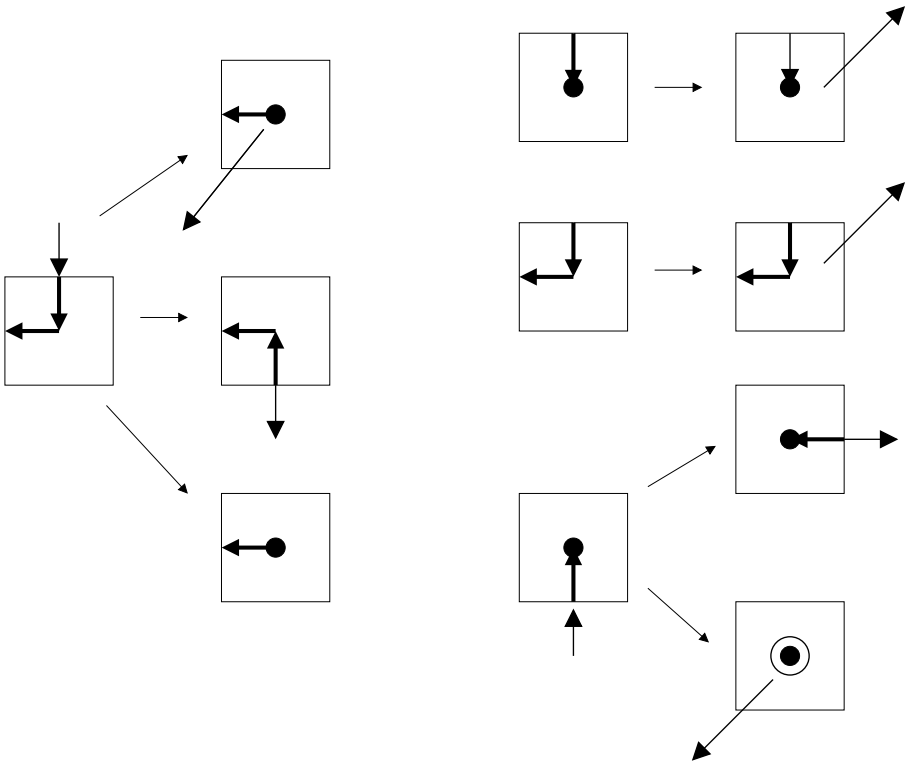

FIG. 3: Examples of the passive update at a site. The absence of an ingoing or an outgoing arrow implies that the update is on the site.

which the site was approached. If $\mu \neq 0$, then after replacing μ with ν, the update moves to the neighboring site $x + \hat{\mu}$ and replaces the backward direction on the new site with zero. Otherwise the update remains on the same site x without disturbing the backward direction on it. Some examples of the active update is shown in Fig.(2). During a *passive update* if the backward direction $\mu \neq 0$, the update ends. Otherwise a new backward direction ν is chosen with probability $w_{\nu,x}/W$. Here $w_{\nu,x} = 0$ if $x + \hat{\nu} \notin \mathcal{C}$, otherwise $w_{\nu=0,x} = c'$, $w_{\nu=\pm 1} = T$ and $w_{\nu,x} = 1$ otherwise. W is the sum of weights of all possible choices. One of the ν is chosen according to heat bath probabilities. When $\nu = 0$ is chosen then either a monomer or an instanton can be created. If the forward direction on the site is non-zero then the probability of creating a monomer is m^2/c' and creating an instanton is c/c' where $c' = c + m^2$. If the forward direction is zero then only an instanton can be created and so $c' = c$. The update ends on a passive site if $\nu = 0$ is chosen with a creation of a monomer. On the other hand

if an instanton is created the update can end only if the forward direction on the site was also zero. Otherwise the update remains on that site and continues. If $\nu \neq 0$ is chosen then the backward direction is changed to ν and the update moves to the neighboring site $x + \hat{\nu}$. Some examples of the passive update is shown in figure 3. Note that in the charged pion directed loop update m^2 is assumed to be zero so monomers can not be generated.

The complete update is simple and is described below.

1. A lattice site $x_0 \in V$ is selected randomly. If x_0 does not belong to $\mathcal{C}$ the whole update ends. Further, if both the forward and the backward directions at this site are non-zero, the site is active and was reached from the $\nu = 0$ direction. Otherwise the site is assumed to be passive.

2. Each current site is updated using the rules of an active site or a passive site successively until the update ends.

Directed path fixed monomer update. This update is identical to the *directed path mass update*, except for a minor change in the *neutral pion directed path update*. The change is such that $\overline{u}u$ or $\overline{d}d$ monomers are not allowed to be created or annihilated during the passive update. Thus, the update allows the monomers to change positions while keeping the total monomer fixed. Note that instanton number can of course change.

V. OBSERVABLES

Numerous observables can be measured with our algorithm. The simplest are the three helicity moduli or current susceptibilities. In particular, for a conserved current $J^i_\mu(x)$, the helicity modulus (current susceptibility) is defined as:

$$Y_i = \frac{1}{dL^d}\left\langle \sum_{\mu=1}^{d} \left(\sum_x J^i_\mu(x) \right)^2 \right\rangle \tag{5}$$

where we are assuming a $L_t \times L^d$ lattice. There are three conserved currents in our model. They are the axial, chiral, and vector currents which are given by:

$$J^a_\mu(x) \;=\; (-1)^x \left[\pi^u_\mu(x) + \pi^d_\mu(x) + |\pi^1_\mu(x)|\right] \tag{6a}$$

$$J^c_\mu(x) \;=\; (-1)^x \left[\pi^u_\mu(x) - \pi^d_\mu(x)\right] \tag{6b}$$

$$J^v_\mu(x) \;=\; \pi^1_\mu(x) \tag{6c}$$

The current susceptibilities Y_a, Y_c and Y_v are diagonal observables in our approach and can be easily computed for every configuration that contributes to the partition function.

We can also measure two point correlation functions of many fermion bilinears. In particular we can compute

$$G^a_\pi(x,y) = \frac{1}{2}\langle\overline{\psi}_x i\sigma^a(-1)^x\psi_x\ \overline{\psi}_y i\sigma^a(-1)^y\psi_y\rangle \tag{7a}$$

$$G_\sigma(x,y) = \frac{1}{2}\langle\overline{\psi}_x\psi_x\ \overline{\psi}_y\psi_y\rangle \tag{7b}$$

$$G_\eta(x,y) = \frac{1}{2}\langle\overline{\psi}_x i(-1)^x\psi_x\ \overline{\psi}_y i(-1)^y\psi_y\rangle \tag{7c}$$

$$G^a_\delta(x,y) = \frac{1}{2}\langle\overline{\psi}_x\sigma^a\psi_x\ \overline{\psi}_y\sigma^a\psi_y\rangle \tag{7d}$$

These correlation functions are non-diagonal observables and cannot be measured easily on the configurations that contribute to the path integral. However, they can be measured during the *charged-pion directed path update* as follows:

1. All the $G_i(x,y)$ are set to zero before the update.

2. If x is the first active site and y is one of the passive sites visited during the directed path update, then $G_i(x,y)$ is changed as follows:

$$G_\pi(x,y) = G_\pi(x,y) + \frac{L_t L^d}{2W_y}\delta_{x,x_0}\delta_{y,y_0} \tag{8a}$$

$$G_\delta(x,y) = G_\delta(x,y) - (-1)^{x+y}\frac{L_t L^d}{2W_y}\delta_{x,x_0}\delta_{y,y_0} \tag{8b}$$

$$G_\sigma(x,y) = G_\pi(x,y) + \frac{L_t L^d}{2W_y}\delta_{x,x_0}\delta_{y,y_0} \tag{8c}$$

$$G_\eta(x,y) = G_\delta(x,y) - (-1)^{x+y}\frac{L_t L^d}{2W_y}\delta_{x,x_0}\delta_{y,y_0} \tag{8d}$$

   If $n_m(z)$ is the number of monomers and $n_I(z)$ is the number of instantons at any lattice site z then the G_η and G_σ correlator get additional "disconnected" contributions:

$$G_\sigma(x,z) = G_\sigma(x,z) + [1 + n_m(z) + 2n_I(z)m^2/\tilde{c}]\frac{L_t L^d}{2W_y} \tag{9a}$$

$$G_\eta(x,z) = G_\eta(x,z) - (-1)^{x+z}[n_m(z) + 2n_I(z)m^2/\tilde{c})]\frac{L_t L^d}{2W_y} \tag{9b}$$

$$\tag{9c}$$

3. The function $G_i(x,y)$ thus obtained for each directed path update, when averaged over directed path updates, yields the final correlation function defined above.

Once the correlation functions are known, the corresponding susceptibilities, χ_π, χ_σ, χ_η and χ_δ are given by:

$$\chi_i = \frac{2}{L^d}\sum_{x,y} G_i(x,y) \tag{10}$$

for $i = \sigma, \pi, \eta, \delta$. We have normalized χ_i such that

$$\chi_i = \frac{1}{L^d}\frac{1}{Z}\frac{\partial^2 Z}{(\partial m)^2} \tag{11}$$

We have tested our algorithm by comparing the results for all the above observables with exact analytic calculations for each of these observables on a 2×2 lattice. The exact results and those from the algorithm are shown in Appendix I.

VI. RESULTS IN THE ϵ-REGIME

In order to establish that we can indeed use our approach to model pions of two flavor QCD, in this paper we focus on the ϵ regime of chiral perturbation theory [22, 23, 24, 25, 26, 27, 28]. In the phase where chiral symmetry is broken and the anomaly is large, the low energy physics of our model must be describable by the Euclidean chiral Lagrangian

$$\mathcal{L} = \frac{F^2}{4}\mathrm{tr}\Big(\partial_\mu U^\dagger \partial_\mu U\Big) - m\Sigma tr\Big(U + U^\dagger\Big) \tag{12}$$

where F is the pion decay constant in the chiral limit and Σ is the chiral condensate and $U \in SU(2)$ is the pion field. The ϵ regime involves the limit where L, the linear size of the four dimensional hypercube, is taken to be large such that $FL \ll 1$ but $m\Sigma L^4$ is held fixed. In this limit a variety of quantities have been computed in the literature. For example the behavior of χ_σ as a function of L at $m = 0$ was obtained in [26] for the $O(N)$ model. The $N = 4$ result, relevant here, is

$$\chi_\sigma = \frac{\Sigma^2 L^4}{4}\left[1 + \frac{3\beta_1}{(FL)^2} + \frac{a}{(FL)^4} + ...\right] \tag{13}$$

The dependence of Y_c and Y_v were obtained in [27] and it was shown that

$$Y_c = \frac{F^2}{2}\left(\left\{1 + \frac{\beta_1}{(FL)^2} + \frac{a'}{(FL)^4} + ...\right\} + \frac{u^2}{24}\left\{1 + \frac{3\beta_1}{(FL)^2} + \frac{b_c}{(FL)^4} + ...\right\} + \mathcal{O}(u^4)\right) \tag{14a}$$

$$Y_v = \frac{F^2}{2}\left(\left\{1 + \frac{\beta_1}{(FL)^2} + \frac{a'}{(FL)^4} + ...\right\} - \frac{u^2}{24}\left\{1 + \frac{3\beta_1}{(FL)^2} + \frac{b_v}{(FL)^4} + ...\right\} + \mathcal{O}(u^4)\right) \tag{14b}$$

for small $u = \Sigma m L^4[1 + 3\beta_1/(2(FL)^2)]$. In the above formulas $\beta_1 = 0.14046$ is the shape coefficient and a,a' b_c,b_v are constants that depend on higher order low energy constants of the chiral expansion. Also note that $Y_c = Y_v$ when $u = 0$ reflects the chiral symmetry of the theory.

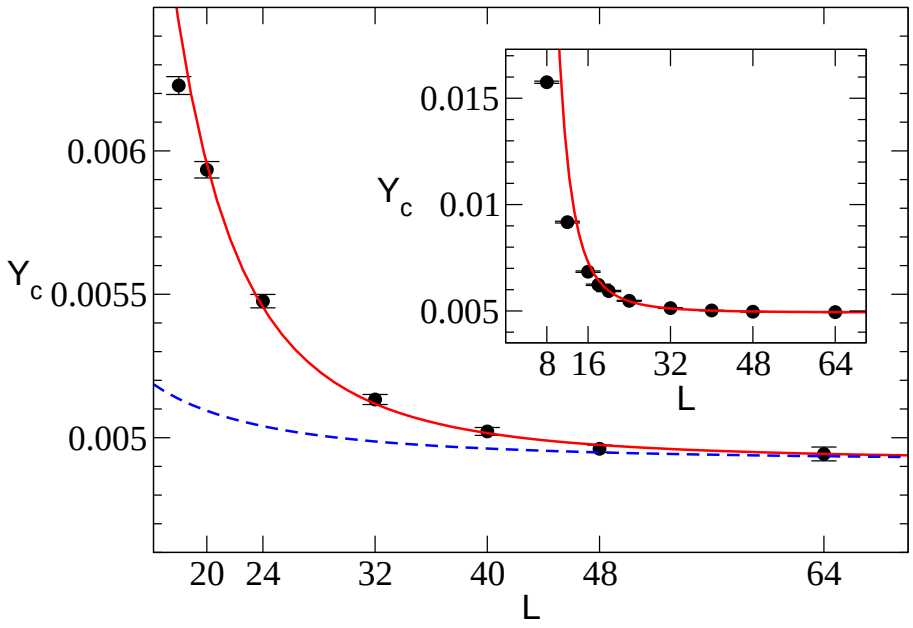

FIG. 4: Vector current susceptibility Y_C as a function of L at $T = 1.733$, $c = 0.3$ and $m = 0$ [$Y_C = Y_V$]. The solid line shows the fit with $F = 0.0992$ and $a' = 2.7$. The dotted line shows the same curve but with $a' = 0$.

We now argue that the calculations in our model are consistent with Eqs.(13) and (14). We choose $c = 0.3$ and $T = 1.733$ with fixed $L_t = 2$. These parameters are chosen so that chiral symmetry is spontaneously broken and the anomalous pion mass (M_η) is about 1 in lattice units. As we will see, this choice of T makes $F \sim 0.1$ in lattice units, which should make our results less sensitive to lattice artifacts. In Fig.(4) we plot our data for Y_c as a function of L for $m = 0$. The solid lines are fits to Eq.(14). The fits are extremely good if we allow for $a' \neq 0$ and use lattice sizes above $L \sim 24$. We can then extract $F = 0.0992(1)$ and $a' = 2.7(1)$ with a $\chi^2/DOF = 0.8$. However, as can be seen from the figure, this means that setting $a' = 0$, i.e.. using only the leading correction in the chiral expansion, will not be a good approximation for $L < 48$. This is clearly due to the smallness of a'/β_1. In

other words, although our data is consistent with the Eq.(14), unfortunately we are not yet sensitive to the universal corrections at order $\mathcal{O}(1/L^2)$.

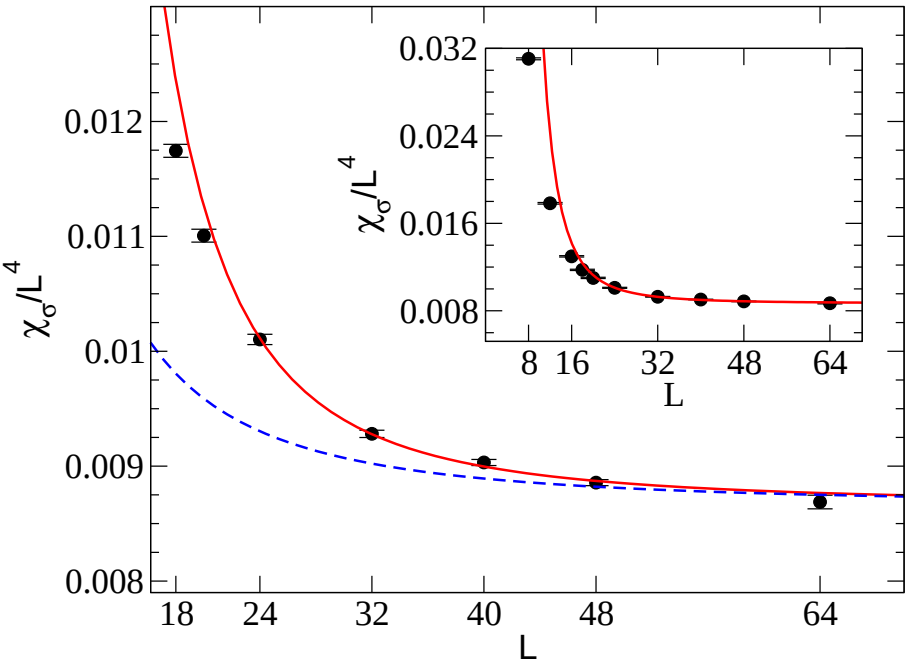

FIG. 5: Chiral condensate susceptibility χ_σ as a function of lattice size L at $T = 1.733$, $c = 0.3$ and $m = 0$ [$\chi_\sigma = \chi_\pi$]. The solid line is the plot of Eq.(13) with $\Sigma = 0.1866$, $F = 0.0992$ and $a = 3.0$. The dotted line shows the same curve but with $a = 0$.

Let us next focus on the condensate susceptibility χ_σ. In Fig(5) we plot χ_σ/L^4 as a function of L. The solid line is a fit to the data using the Eq.(13) where we fix $F = 0.0992$ and take only the data for $L > 20$ in the fit. We find $\Sigma = 0.1862(2)$, $a = 3.0(2)$ with a $\chi^2/DOF = 1.3$. As can be seen again, the universal correction at order $\mathcal{O}(1/L^2)$ is small compared to the next order non-universal correction for $L < 48$.

In the current work we neglect the $\log(L)$ corrections that arise at the order $1/(FL)^4$ [3]. The reason is as follows: Consider for example the chiral condensate susceptibility defined Eq. (11). Using the results of [3, 4, 26], we can obtain the logarithmic corrections to Eq. (13). In particular we find that

$$\chi_\pi = \frac{\Sigma^2 L^4}{4}\left[1 + \frac{3\beta_1}{F^2L^2} + \frac{1}{F^4L^4}\Big\{\alpha + \frac{15}{16\pi^2}(\log FL)\Big\} + O\big(\frac{1}{F^5L^5}\big)\right] \tag{15}$$

where now $\alpha = (3\beta_1^2 + 15\beta_2)/2 + 3[\log(\Lambda_M/F) + 4\log(\Lambda_\Sigma/F)]/16\pi^2$ and $\beta_2 = -0.020305$ is another shape coefficient. The mass scales $\Lambda_M, \Lambda_\Sigma$ encode the non-universal information of our model and are defined in [26]. Assuming $L_1 = 20$ is the smallest lattice size and $L_2 = 64$ is the largest lattice size we use in the fits, we see that the change in the logarithmic correction term $15\log(L_2/L_1)/(16\pi^2) \sim 0.1$ is within errors of the constant $a = 3.0(2)$ obtained above by fitting the χ_π data to Eq.(13). Thus, we believe our errors are still large and we are not yet sensitive to the logarithmic corrections. Interestingly, since $15\log(FL)/(16\pi^2)$ is much smaller than a in the region of our fits, we can estimate that $a \sim 3[\log(\Lambda_M/F) + 4\log(\Lambda_\Sigma/F)]/(16\pi^2)$, which means that $[\log(\Lambda_M/F) + 4\log(\Lambda_\Sigma/F)]$ (~ 150) is unnaturally large, and the factor $\frac{1}{16\pi^2}$ is essential to keep the coefficient of $1/(FL)^4$ of order 1. In other words factors like $\frac{1}{16\pi^2}$ cannot always be assumed to be small since they can be multiplied by large numbers.

Having confirmed that our results are consistent with Eq.(14) when $u = 0$, we can also check that our model gives results consistent with Eq.(14) at order u^2. One way to do this is to tune the quark mass and the volume such that u is fixed and small. This is cumbersome. For example even at $u = 1$ we see that for $L = 48$ our quark mass should be as small as 10^{-6}. Since m^2 is involved in a probability, one begins to worry about double precision arithmetic. Thus, here we devise another method. To understand our approach let us expand the partition function in powers of the quark mass

$$Z = Z_0 + m^2 Z_2 + m^4 Z_4 + ... \tag{16}$$

where Z_n is obtained from configurations with n monomers. In this expansion we can neglect the m^2 contribution to instanton weights as they will not contribute in the ϵ regime. Similarly, let $Y_v^{(n)}$ and $Y_c^{(n)}$ be the value of the current susceptibilities when computed in the n monomer sector. Expanding observables in the various monomer sectors it is possible to show

$$Y_i = Y_i^{(0)} + m^2 \left\{ Y_i^{(2)} - Y_i^{(0)} \right\} \frac{Z_2}{Z_0} + ... \tag{17}$$

where $i = v, c$. From Eq.(13) we see that

$$\frac{Z_2}{Z_0} = \Sigma^2 \frac{L^{2d}}{8} \left(1 + \frac{3\beta_1}{(FL)^2} + \frac{a}{(FL)^4} + ... \right) \tag{18}$$

Since at $u = 0$ no monomers contribute we also have

$$Y_i^{(0)} = \frac{F^2}{2}\left(1 + \frac{\beta_1}{(FL)^2} + \frac{a'}{(FL)^4} + ...\right) \tag{19}$$

Substituting our knowledge of Z_2/Z_0 and Y_c^0 we get

$$Y_i = \left(\frac{F^2}{2}\left\{1 + \frac{\beta_1}{(FL)^2} + ...\right\} + \frac{u^2}{8}\left\{Y_i^{(2)} - Y_i^{(0)}\right\} + ...\right) \tag{20}$$

Comparing with Eq.(14) we conclude that

$$Y_c^{(2)} = \frac{2F^2}{3}\left(1 + \frac{3\beta_1}{2(FL)^2} + \frac{b'_c}{(FL)^4} + ...\right) \tag{21a}$$

$$Y_v^{(2)} = \frac{F^2}{3}\left(1 + \frac{b'_v}{(FL)^4} + ..\right) \tag{21b}$$

Notice that $Y_c^{(2)} \neq Y_v^{(2)}$ due to the effects of explicit chiral symmetry breaking that is introduced due to the presence of the monomers.

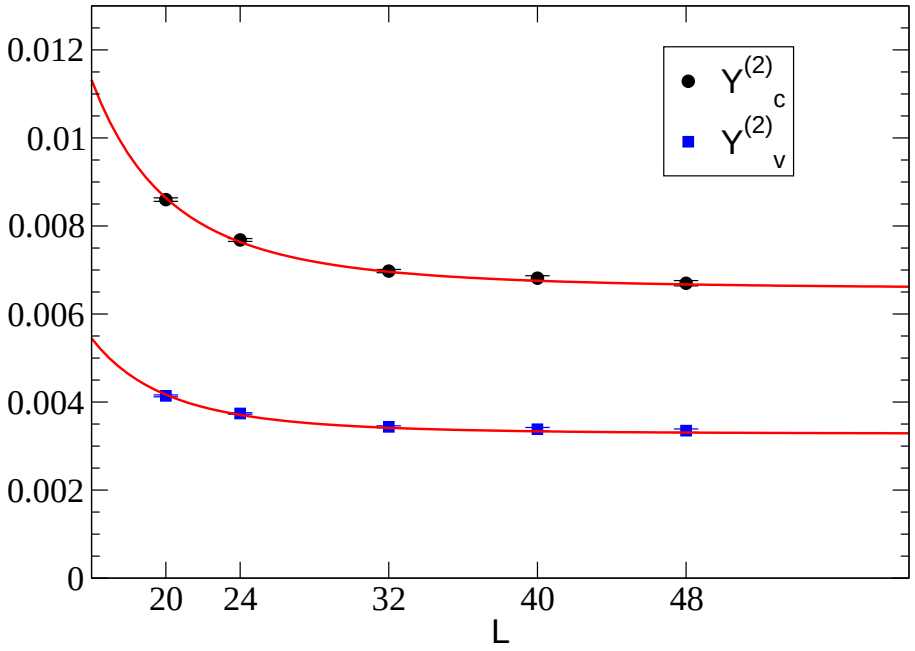

FIG. 6: Plot of $Y_c^{(2)}$ and $Y_v^{(2)}$, evaluated in the two monomer sector as a function of L at $T = 1.733$, $c = 0.3$ and $m = 0$. The solid lines are fits to Eq. (21) discussed in the text.

We have used the fixed monomer update to compute $Y_c^{(2)}$ and $Y_v^{(2)}$. In Fig.(6) we plot our results as a function of L. We fix $F = 0.0992$ and try to fit our data to Eq.(21). We obtain $b'_c = 4.1(1)$ with a $\chi^2/DOF = 1.1$, and $b'_v = 4.2(1)$ with a $\chi^2/DOF = 2.1$. Although our results again appear consistent with the predictions at large L, the large values for the constants b'_c and b'_v show that we need data with small errors for $L > 48$ to be sure we can be sensitive to the universal predictions at $\mathcal{O}(1/L^2)$.

While our model is analogous to real QCD, we can not expect our results to be equivalent to real QCD. However, for pedagogical reasons, we can make comparisons to real QCD studies. In particular, at $T = 1.733$, we found $Fa_{\rm lat} = 0.0992$ and $M_\eta a_{\rm lat} = 1.1$ where we have introduced $a_{\rm lat}$ to be the lattice spacing. If we take $a_{\rm lat} = 1GeV^{-1}$, we find $F \sim 99$MeV and $M_\eta \sim 1.1$GeV which are reasonably close to physical values.

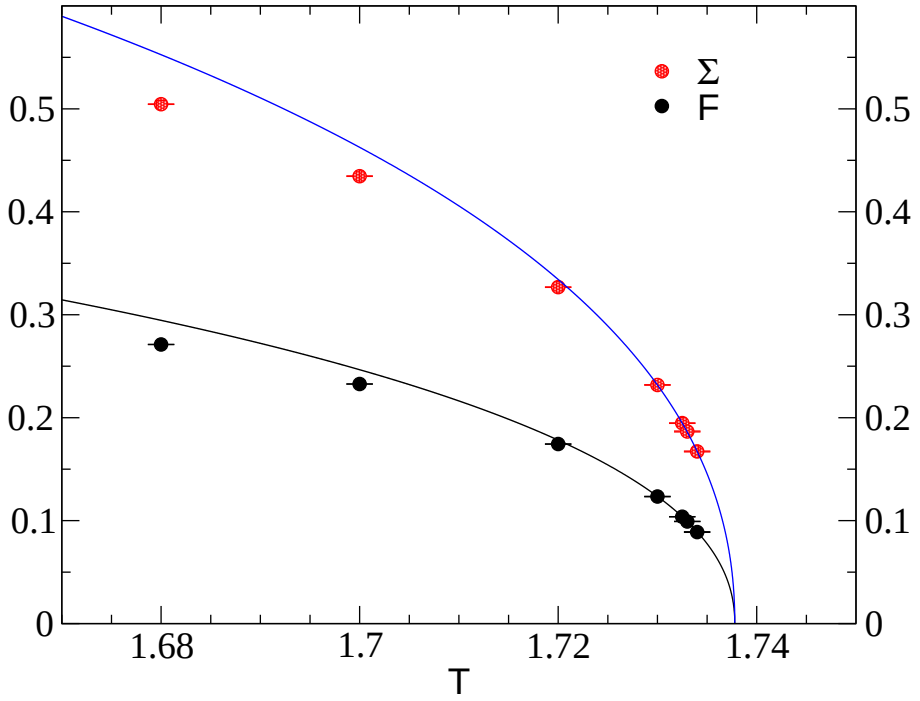

FIG. 7: F and Σ plotted as a function of T. The solid lines are fits to Eq.(22) with $A_F = 0.943$, $A_\Sigma = 1.769$ and $T_c = 1.73779$.

VII. CONTINUUM LIMIT

At $c = 0.3$ and $T = 1.733$ we found that $F \sim 0.1$. Such a small value of F clearly is not an accident. At a fixed $c \neq 0$ the model should go through a phase transition at some

T	F	a	χ^2	Σ	b	χ^2	M_η	χ^2
1.68	0.2711(1)	1.28(3)	0.3	0.5045(2)	1.22(4)	1.1	1.04(5)	1.5
1.70	0.2327(1)	1.91(9)	1.2	0.4346(2)	1.72(11)	0.2	1.06(5)	1.2
1.72	0.1744(1)	2.58(13)	0.1	0.3268(2)	2.44(17)	0.5	1.02(3)	1.1
1.73	0.1234(2)	2.25(10)	1.7	0.2318(2)	2.26(8)	1.5	1.05(2)	1.6
1.7325	0.1038(1)	2.80(18)	0.1	0.1947(2)	2.77(23)	0.7	1.08(3)	1.3
1.733	0.0992(1)	2.71(9)	0.8	0.1866(4)	3.00(20)	1.8	1.05(3)	1.5
1.734	0.0889(3)	2.78(15)	2.3	0.1672(4)	2.81(17)	2.3	1.08(3)	1.4

TABLE I: Fits of Y_c and χ_σ as a function of L based on Eqs. (14) and (13) at $c = 0.3$ and $m = 0$ at various values of $T < T_c$. The last two columns give the value M_η and the χ^2/DOF obtained from a fit to $G_\eta(x, y)$.

critical temperature T_c. If this transition is second order then at the critical temperature one would expect F to vanish. Thus, $T = 1.733$ must be close to such a critical point. Since we are in four dimensions, we expect quantities to obey mean field scaling near a second order critical point. In particular this means [29]:

$$F \sim A_F (T_c - T)^{\frac{1}{2}} |\log(T_c - T)|^{\frac{1}{4}} \tag{22a}$$

$$\Sigma \sim A_\Sigma (T_c - T)^{\frac{1}{2}} |\log(T_c - T)|^{\frac{1}{4}} \tag{22b}$$

We have verified that our results for $c = 0.3$ are consistent with this expectation. Tab.(I) gives the chiral perturbation theory fit parameters as a function of T. The values of F and Σ are plotted as a function of T in Fig.(7). If we use the data for $T \geq 1.73$ a combined fit of F and Σ as a function of T to Eq.(22) gives $A_F = 0.943(4)$, $A_\Sigma = 1.769(4)$ and $T_c = 1.73779(4)$ with a $\chi^2/DOF = 0.7$.

Although we cannot rule out a weak first order transition with a large correlation length, if we assume that there is a second order critical point at $T = T_c$, we can in principle make F arbitrarily small by tuning our T closer and closer to T_c. This raises an interesting question: By approaching T_c can we define a "continuum limit" of our lattice pion theory by holding F to be the fixed physical scale? However, due to triviality of four dimensional scalar field theories this limiting theory is expected to be free [30, 31, 32]. On the other hand, chiral perturbation theory suggests that pions will always interact as their momentum increases

which is in contradiction to the statement of triviality. Hence, we conjecture that the mass of the σ resonance will go to zero in units of F. Since triviality is a logarithmic effect we expect $M_\sigma/F \sim 1/|\log(T_c - T)]|^p$ where p is some power. This means that the chiral expansion would break down at momenta close to M_σ rather than F and the usual power counting of chiral perturbation theory would become questionable close to T_c. Thus, our approach to model pion physics of QCD should eventually fail! On the other hand since triviality is a logarithmic effect, it is likely that we still will have a window where our model produces pions very much like in two-flavor QCD. The present study is an attempt to demonstrate this in the ϵ-regime.

VIII. CONCLUSIONS AND FUTURE WORK

In this work we have developed a new approach to model the physics of pions in $N_f = 2$ QCD. Our approach uses $N_f = 2$ lattice QED in the strong coupling limit. We have shown that using the mapping to dimer models we can study our model very efficiently in the chiral limit and close to it. We have established consistency with the ϵ regime predictions of chiral perturbation theory. We have also demonstrated that we can make $F \ll 1$ by tuning a fictitious temperature so one approaches a second order phase transition. This tuning is expected to help remove lattice artifacts and approach a *continuum-like* theory. But, as explained in section VII, our method will eventually fail due to logarithmic triviality of scalar field theories. Since triviality is a logarithmic effect, there should be a large window where our method may provide a model for pions. Our results confirm this belief.

There are many directions for the future. We are currently performing calculations in the p-regime and hope to understand the region in our model where chiral perturbation theory, up to a particular order, will be valid [33, 34, 35, 36, 37, 38, 39, 40]. Since we have already computed the leading low energy constants in the ϵ-regime we can constrain them when we analyze the p-regime. Another interesting arena to explore is pion scattering and resonance physics by measuring the appropriate two and four point correlation functions and extracting scattering lengths and phase shifts via Lüscher's method [41, 42]. Our approach should also allow one to study the effects of the quark mass on these quantities.

Acknowledgments

DJC gratefully achnowledges B.C. Tiburzi and F.J. Jiang for discussions relevant to this work. SC thanks Gilberto Colangelo, Stephan Dürr, and Uwe-Jens Wiese for discussions and hospitality at Bern University where part of this work was done. DJC also acknowledges Robert G. Brown for technical assistance in C programming. This work was partially supported by the DOE grant DE-FG02-05ER41368.

---

[1] L. Giusti, PoS. **LAT2006** (2007), hep-lat/0702014.

[2] C. T. Sachrajda, AIP Conf. Proc. **842**, 198 (2006), hep-lat/0601014.

[3] M. Gockeler, K. Jansen, and T. Neuhaus, Phys. Lett. **B273**, 450 (1991).

[4] A. Hasenfratz et al., Nucl. Phys. **B356**, 332 (1991).

[5] A. Hasenfratz et al., Z. Phys. **C46**, 257 (1990).

[6] B. B. Beard and U. J. Wiese, Phys. Rev. Lett. **77**, 5130 (1996), cond-mat/9602164.

[7] S. Chandrasekharan and A. C. Mehta (2006), hep-lat/0611025.

[8] J. M. Blairon, R. Brout, F. Englert, and J. Greensite, Nucl. Phys. **B180**, 439 (1981).

[9] N. Kawamoto and J. Smit, Nucl. Phys. **B192**, 100 (1981).

[10] H. Kluberg-Stern, A. Morel, and B. Petersson, Nucl. Phys. **B215**, 527 (1983).

[11] O. Martin and B. Siu, Phys. Lett. **B131**, 419 (1983).

[12] E. Dagotto, A. Moreo, and U. Wolff, Phys. Lett. **B186**, 395 (1987).

[13] E. Dagotto, A. Moreo, and U. Wolff, Phys. Rev. Lett. **57**, 1292 (1986).

[14] E. Dagotto, F. Karsch, and A. Moreo, Phys. Lett. **B169**, 421 (1986).

[15] F. Karsch and K. H. Mutter, Nucl. Phys. **B313**, 541 (1989).

[16] J. U. Klatke and K. H. Mutter, Nucl. Phys. **B342**, 764 (1990).

[17] G. Boyd, J. Fingberg, F. Karsch, L. Karkkainen, and B. Petersson, Nucl. Phys. **B376**, 199 (1992).

[18] D. H. Adams and S. Chandrasekharan, Nucl. Phys. **B662**, 220 (2003), hep-lat/0303003.

[19] D. J. Cecile (2006), hep-lat/0611026.

[20] P. Rossi and U. Wolff, Nucl. Phys. **B248**, 105 (1984).

[21] S. Chandrasekharan and F.-J. Jiang, Phys. Rev. **D74**, 014506 (2006), hep-lat/0602031.

[22] H. Neuberger, Phys. Rev. Lett. **60**, 889 (1988).

[23] H. Neuberger, Nucl. Phys. **B300**, 180 (1988).

[24] J. Gasser and H. Leutwyler, Phys. Lett. **B188**, 477 (1987).

[25] J. Gasser and H. Leutwyler, Nucl. Phys. **B307**, 763 (1988).

[26] P. Hasenfratz and H. Leutwyler, Nucl. Phys. **B343**, 241 (1990).

[27] F. C. Hansen and H. Leutwyler, Nucl. Phys. **B350**, 201 (1991).

[28] F. C. Hansen, Nucl. Phys. **B345**, 685 (1990).

[29] J. Zinn-Justin, *Quantum Field Theory and Critical Phenomena* (Oxford University Press, Oxford, 4th Edition, (2004)).

[30] M. Luscher and P. Weisz, Nucl. Phys. **B295**, 65 (1988).

[31] M. Luscher and P. Weisz, Nucl. Phys. **B318**, 705 (1989).

[32] J. Balog, A. Duncan, R. Willey, F. Niedermayer, and P. Weisz, Nucl. Phys. **B714**, 256 (2005), hep-lat/0412015.

[33] J. Bijnens, G. Colangelo, and P. Talavera, JHEP **05**, 014 (1998), hep-ph/9805389.

[34] G. Colangelo, S. Durr, and R. Sommer, Nucl. Phys. Proc. Suppl. **119**, 254 (2003), hep-lat/0209110.

[35] G. Colangelo and S. Durr, Eur. Phys. J. **C33**, 543 (2004), hep-lat/0311023.

[36] G. Colangelo, Nucl. Phys. Proc. Suppl. **140**, 120 (2005), hep-lat/0409111.

[37] G. Colangelo and C. Haefeli, Phys. Lett. **B590**, 258 (2004), hep-lat/0403025.

[38] G. Colangelo, A. Fuhrer, and C. Haefeli, Nucl. Phys. Proc. Suppl. **153**, 41 (2006), hep-lat/0512002.

[39] G. Colangelo, S. Durr, and C. Haefeli, Nucl. Phys. **B721**, 136 (2005), hep-lat/0503014.

[40] G. Colangelo and C. Haefeli, Nucl. Phys. **B744**, 14 (2006), hep-lat/0602017.

[41] M. Luscher, Nucl. Phys. **B354**, 531 (1991).

[42] S. R. Beane, P. F. Bedaque, K. Orginos, and M. J. Savage (NPLQCD), Phys. Rev. **D73**, 054503 (2006), hep-lat/0506013.

Appendix I

Here we give the analytic expressions for the partition function, the chiral, vector, and axial helicity moduli and the two susceptibilities for a 2×2 lattice,as defined in Section(V). (Note $c = \tilde{c} + m^2$):

$$\begin{aligned}
Z(T,c,m) &= 36T^4 + 64T^2 + 36 + c^4 + 12(1+T^2)c^2 + 8(1+T)c^2m^2 && \text{(23a)}\\
&+ 32Tcm^2 + 16(1+T^2)m^4 + 48(1+T^3)m^2 + 32(T+T^2)m^2 \\
2Z \times Y_W^C(T,c,m) &= 96 + 64T^2 + 16c^2 + 112m^2 + 32m^4 + 8c^2m^2 + 32Tcm^2 && \text{(23b)}\\
&+ 32(2T+T^2)m^2 \\
2Z \times Y_W^V(T,c,m) &= 96 + 64T^2 + 16c^2 + 64m^2 && \text{(23c)}\\
Y_W^A(T,c,m) &= Y_W^C(T,c,m) + \frac{64T^2m^2}{2Z} && \text{(23d)}\\
2Z \times \chi_\pi &= 24T^3 + 16T^2 + 16T + 24 + 4(1+T)c^2 + 4(3+4T+3T^2)c + 2c^3 && \text{(23e)}\\
&+ 8(1+T)cm^2 + 16(1+T+T^2)m^2 \\
2Z \times \chi_\eta &= 24T^3 + 16T^2 + 16T + 24 + 4(1+T+m^2)c^2 - 4(3-4T+3T^2)c && \text{(23f)}\\
&- 2c^3 - 8(1+T)cm^2 + 8(5+6T+5T^2)m^2 + 16(1+T)m^4
\end{aligned}$$

In Tabs.(II) and (III) we compare the analytic results with the results obtained using our algorithm for different parameters. The agreement gives us confidence that our algorithm must be correct.

T	c	m	*Algo.*	*Exact*	*Algo.*	*Exact*	*Algo.*	*Exact*
			Y_w^A		Y_w^C		Y_w^V	
1.0	0.5	0.0	0.8023(9)	0.80246...	0.5763(6)	0.57721...	0.5771(8)	0.57721...
1.5	0.5	0.0	0.5212(7)	0.52141...	0.3275(6)	0.32790...	0.3274(7)	0.32790...
1.0	1.0	0.0	0.7449(8)	0.74534...	0.5470(7)	0.54658...	0.5468(8)	0.54658..
1.5	1.0	0.0	0.4967(7)	0.49720...	0.3178(5)	0.31821...	0.3175(6)	0.31821...
1.0	1.5	0.0	0.6667(8)	0.66645...	0.5016(5)	0.50240...	0.5014(6)	0.50240...
1.5	1.5	0.0	0.4607(6)	0.46147...	0.3029(5)	0.30325...	0.3033(6)	0.30325...
1.0	2.0	0.0	0.5812(7)	0.58064...	0.4519(6)	0.45161...	0.4521(6)	0.45161...
1.5	2.0	0.0	0.4199(5)	0.41927...	0.2853(5)	0.28451...	0.2853(5)	0.28451...
1.0	0.0	0.5	0.7734(5)	0.77336...	0.5972(5)	0.59730...	0.4867(6)	0.48692...
1.5	0.0	0.5	0.5062(6)	0.50702...	0.3479(5)	0.34834...	0.2827(4)	0.28319...
1.25	0.5	1.5	0.4192(4)	0.41948...	0.3914(6)	0.39164...	0.1285(3)	0.12831...
1.5	1.25	0.5	0.4516(5)	0.45126...	0.3250(4)	0.32496...	0.2564(4)	0.25611...
2.0	1.25	1.5	0.2664(3)	0.26636...	0.2395(3)	0.23928...	0.0733(1)	0.07318...
1.0	0.5	2.0	0.3834(5)	0.38411...	0.3757(4)	0.37622...	0.0915(2)	0.09122

TABLE II: Helicity moduli for a 2×2 lattice as discussed in the text.

			χ_π		χ_η	
T	c	m	*Algo.*	*Exact*	*Algo.*	*Exact*
1.0	0.5	0.0	0.3601(3)	0.359877...	0.2172(2)	0.217334...
1.5	0.5	0.0	0.2676(2)	0.267764...	0.1824(1)	0.182429...
1.0	1.0	0.0	0.4040(3)	0.403727...	0.1429(2)	0.142857...
1.5	1.0	0.0	0.2981(2)	0.298322...	0.1367(1)	0.136731...
1.0	1.5	0.0	0.4220(3)	0.422301...	0.0801(1)	0.080103...
1.5	1.5	0.0	0.3172(3)	0.317264...	0.0948(1)	0.094767...
1.0	2.0	0.0	0.4194(2)	0.419355...	0.0323(1)	0.032258...
1.5	2.0	0.0	0.3251(3)	0.324754...	0.0588(1)	0.058961...
1.0	0.0	0.5	0.2849(2)	0.28481...	0.2849(2)	0.28481...
1.5	0.0	0.5	0.2220(1)	0.22220...	0.2220(1)	0.22220...
1.25	0.5	1.5	0.1708(2)	0.17081...	0.1412(2)	0.14121...
1.5	1.25	0.5	0.2767(2)	0.27650...	0.1175(1)	0.11753...
2.0	1.25	1.5	0.1384(1)	0.13831...	0.0933(1)	0.09323...
1.0	0.5	2.0	0.1339(1)	0.13365...	0.1160(1)	0.11584...

TABLE III: Susceptibilities for a 2×2 lattice as discussed in the text.